Supporting Information

Controllable synthesis of MoS_2@TiO_2 Nanocomposites for Visual detection of Dopamine Secretion with Highly-efficient Enzymatic Activity

Chong Hui Wei[a], Xuan Xie[b], Yue Mou[a], Shiqi Cheng[a], Jing Yang[a], Kaixin Xue[a], Kewei Yu[a], Xinru Lin[a], Chunfen Zhang[a], YuJie Zhao[b]*, Xingyu Luo[a]*, Yilin Wang[a]

[a]School of Chemistry and Chemical Engineering, Guangxi University, Nanning 530004, P.R. China.

[b]State Key Laboratory of Chemo/Biosensing and Chemometrics, College of Chemistry and Chemical Engineering, Hunan University, Changsha, 410082, P. R. China.

*Corresponding authors: jamesluoxingyu@163.com (Xingyu Luo); zhaoyujiehnu@163.com (Yujie Zhao)

Contents

Additional Experimental Procedures

Cell culture. SH-SY5Y cells were cultured in colorless DMEM (Gibco) supplemented with 10% (v/v) FBS (Gibco), penicillin (100 U/mL) and streptomycin (100 μg/mL). All cells were maintained at 37 ℃ with 5% CO_2 in a humidified atmosphere.

Time-lapse confocal imaging. About 10^5 SH-SY5Y cells were cultured in the 35 mm confocal dish in complete medium at 5% CO_2 and 37 °C for another 24 h incubation. 5 μM Fluo-8 were firstly added into the cells for 20 minutes incubation at 37 °C and then washed by PBS buffer for three times. Confocal dish was transferred and fastened under a confocal laser scanning microscope, then the high-K^+ buffer (80 mM KCl, 2 mM $CaCl_2$, 50 mM NaCl, 0.7 mM $MgCl_2$, 1 mM NaH_2PO_4, and 10 mM HEPES) was added into the dish for another 60 s stimulation. The time-lapse imaging was performed using a 488 nm laser for the excitation of Fluo-8. The fluorescence was collected at the corresponding fluorescent channels consecutively with an interval of 60 s and the images were processed using ImageJ software.

Optimization of MoS_2@TiO_2 NCs catalysis. For optimizing the concentration of MoS_2@TiO_2 NCs, different concentration of MoS_2@TiO_2 NCs ranging from 0.005 to 0.0275 mg/mL, 20 μL H_2O_2 (1 M), and 200 μL TMB (10 mM) were mixed in a 2 mL reaction buffer (1×, 0.1 M citrate-sodium citrate, pH 4.0). For optimizing the concentration of TMB, different concentration of TMB ranging from 0.25 to 1.4 mM, 20 μL H_2O_2 (1 M), and 90 μL MoS_2@TiO_2 NCs (0.5 mg/mL) were mixed in a 2 mL reaction buffer (1×, 0.1 M citrate-sodium citrate, pH 4.0). For optimizing the concentration of H_2O_2, different concentration of H_2O_2 ranging from 0 to 35 mM, 200 μL TMB (10 mM), and 90 μL MoS_2@TiO_2 NCs (0.5 mg/mL) were mixed in a 2 mL reaction buffer (1×, 0.1 M citrate-sodium citrate, pH 4.0). The pH optimization of reaction solution is measured under the optimal reaction conditions. In particular, $\Delta Abs=A_1-A_0$, A_1 represents the maximum absorbance at the wavelength of 652 nm, A_0 represents the background absorbance at the wavelength of 652 nm. All reaction solutions were incubated at 30 ℃ for 30 minutes and recorded by UV-4802 spectrophotometer.

EPR measurement. 90 μL MoS_2@TiO_2 NCs (0.5mg/mL) with or without 200 μM DA were mixed with the 10 mM H_2O_2 and 300 mM DMPO in a 2 mL reaction buffer (1×, 0.1 M citrate-sodium citrate, pH 4.0) for 10 min incubation. All Spectrum was

recorded by using the EPR spectrometer A300-10/12 (Bruker, German).

Neurotransmitter interference analysis. 90 μL MoS_2@TiO_2 NCs (0.5 mg/mL), 40 μL DA (10 mM) and 40 μL other neurotransmitters (10 mM) were mixed with 20 μL H_2O_2 (1 M) and 200 μL TMB (10 mM) in 2 mL reaction buffer (1×, 0.1 M citrate-sodium citrate, pH 4.0). The mixtures were incubated at 30 ℃ for 30 min and then recorded the absorption value at the wavelength of 652 nm by UV-4802 spectrophotometer (Unico Co., Ltd., Shanghai, China).

Table S1. Comparison of steady state kinetics with MoS_2 and natural enzyme HRP**.**

Catalyst	Substance	K_m [mM]	V_{max} [Ms^{-1}]	Reference
HRP	TMB	3.95	37.7×10^{-8}	(Feng et al. 2013)
	H_2O_2	10.4	0.689×10^{-8}	
MoS_2	TMB	0.88	1.13×10^{-8}	Present work
	H_2O_2	7.85	1.04×10^{-8}	
MoS_2@ TiO_2 NCs	TMB	0.56	2.31×10^{-8}	Present work
	H_2O_2	2.77	1.90×10^{-8}	

Table S2. Comparison with reported colorimetric methods for DA detection.

Material	Methods	Linear range (μM)	LOD (μM)	Reference
Por-$CuCo_2O_4$	Colorimetry	0-100	0.94	(He et al. 2021)
AHMT-AuNPs	Colorimetry	0.20-1.10	0.07	(Fan et al. 2016)
Silver nanoparticles	Colorimetry	0.2-30	0.2	(Rithesh Raj et al. 2016)
Cu–Mn–O/C-dots	Colorimetry	0-75	0.5	(Wang et al. 2019)
Pt/$CoSn(OH)_6$ NCs	Colorimetry	5-60	0.76	(Liu et al. 2019)
$Ru_{0.3}Co_{2.7}O_4$ NPs	Colorimetry	0-16	0.1	(Wen et al. 2022)
MoS_2@TiO_2 NCs	Colorimetry	0-100	0.194	present work

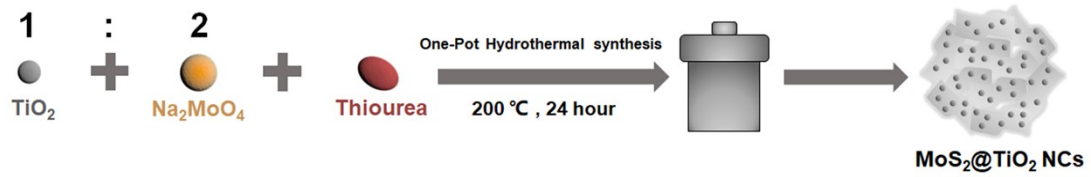

Scheme S1. Schematic illustration of the one-pot hydrothermal procedure for MoS_2@TiO_2 NCs preparation.

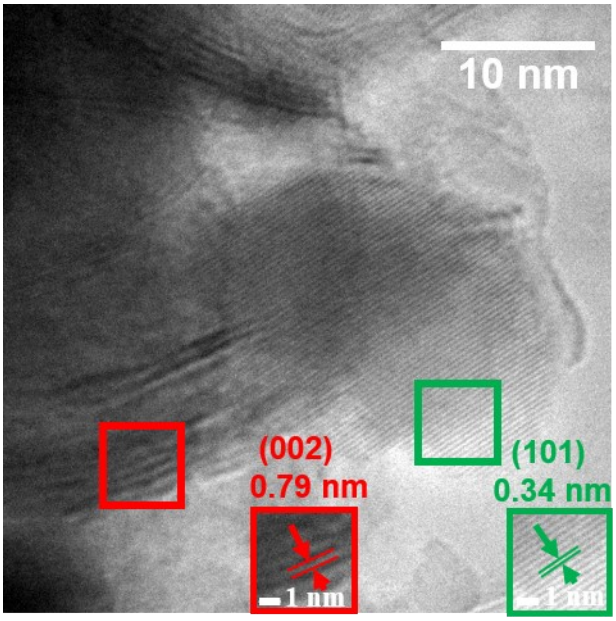

Figure S1. High-resolution TEM images for the lattice distance of TiO_2 and MoS_2, the scale bar of insert image: 1 nm. The scale bar for TEM image is 10 nm.

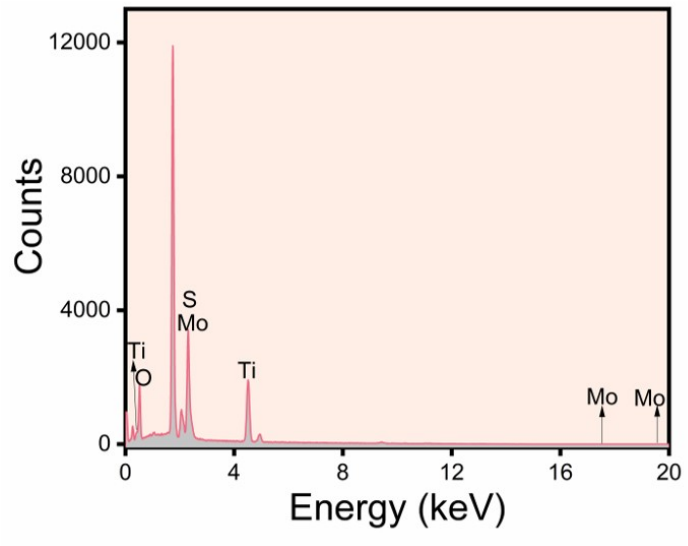

Figure S2. (A) EDS characterization for elements verification in MoS_2@TiO_2 NCs.

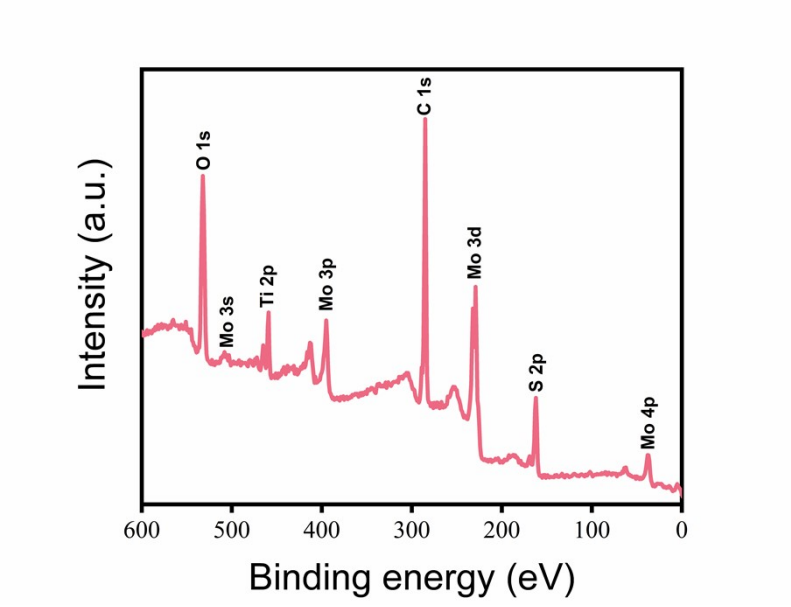

Figure S3. The XPS full pattern of MoS_2@TiO_2 NCs.

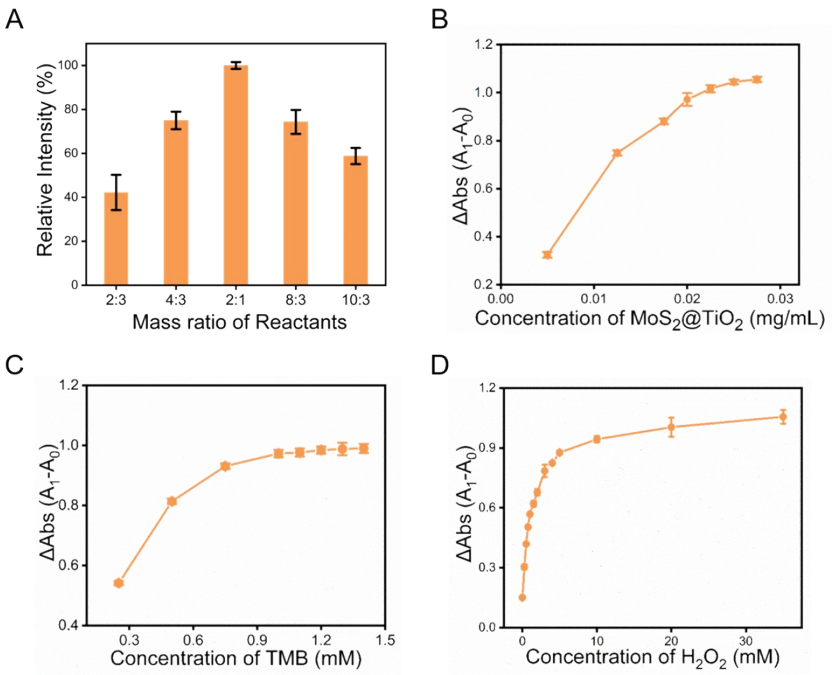

Figure S4. Optimization experiments for (A) the comparison of the catalytic activities with different mass ratio of the reactants between $Na_2MoO_4 \cdot 2H_2O$ and TiO_2. (B) the concentration of $MoS_2@TiO_2$ NCs ranging from 0.005 to 0.0275 mg/mL. (C) the concentration of TMB ranging from 0.25 to 1.4 mM. (D) the concentration of H_2O_2 ranging from 0 to 35 mM.

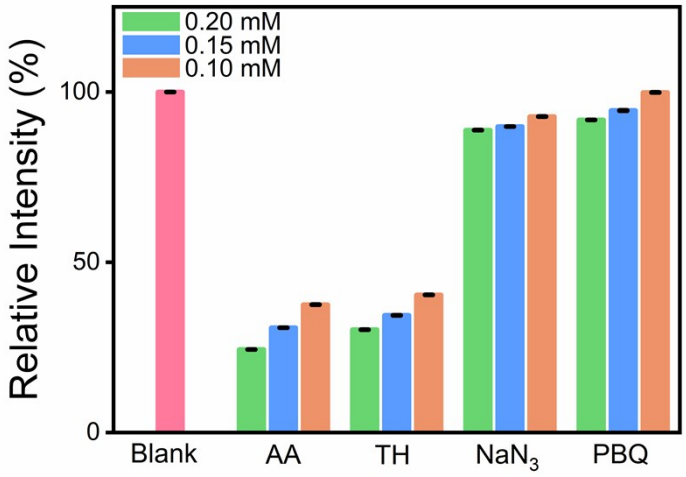

Figure S5. The $MoS_2@TiO_2$ NCs catalysis at the presence of different radical scavengers. Different concentration of radical scavengers including AA, TH, NaN_3 and PBQ were mixed with 90 μL $MoS_2@TiO_2$ NCs (0.5 mg/mL), 20 μL H_2O_2 (1 M) and 200 μL TMB (10 mM) in a 2 mL reaction buffer (1×, 0.1 M citrate-sodium citrate, pH 4.0). Each absorbance at 652 nm was recorded to calculate the scavenging efficiency, respectively.

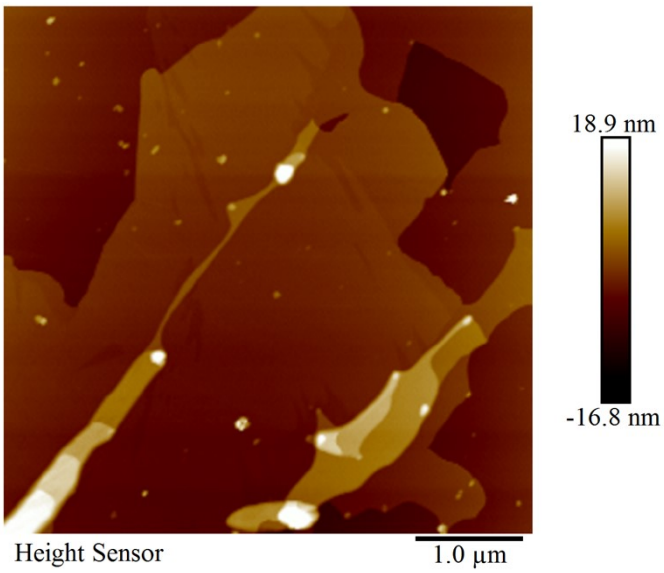

Figure S6. The atomic force microscope (AFM) image of synthesized sheet-like MoS_2 with the same procedure.

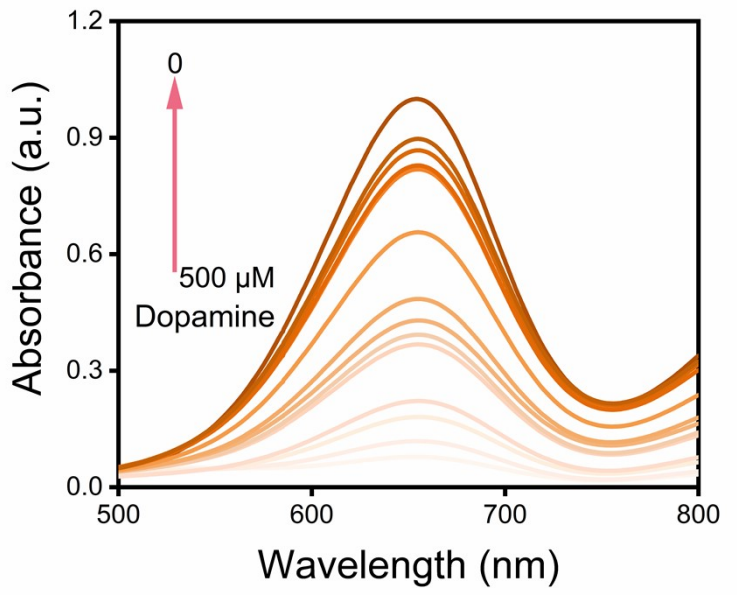

Figure S7. The UV-vis titration spectrum of TMB oxidation by MoS_2@TiO_2 NCs catalysis with different concentrations of DA.

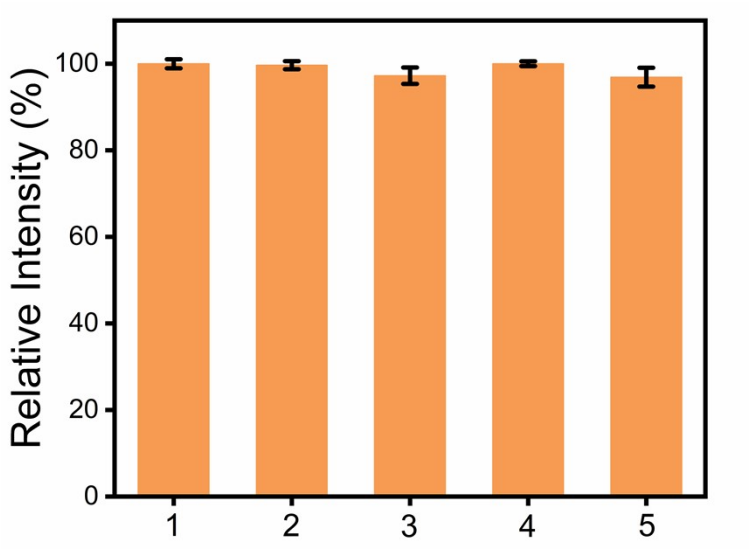

Figure S8. The relative intensity of MoS_2@TiO_2 NCs catalysis in different solution environment with the same concentration of H_2O_2 10 mM, TMB 1 mM, 90μL MoS_2@TiO_2 NCs (0.5 mg/mL). **1**: Blank (in citrate-sodium citrate buffer), **2**: Colorless medium, **3**: High-K^+ buffer (80 mM KCl, 2 mM $CaCl_2$, 50 mM NaCl, 0.7 mM $MgCl_2$, 1 mM NaH_2PO_4, and 10 mM HEPES), **4**: Reaction buffer without K^+ (2 mM $CaCl_2$, 50 mM NaCl, 0.7 mM $MgCl_2$, 1 mM NaH_2PO_4, and 10 mM HEPES). **5**: PBS buffer (1×, 4.2 mM KCl, 2 mM $CaCl_2$, 140 mM NaCl, 0.7 mM $MgCl_2$, 1 mM NaH_2PO_4).

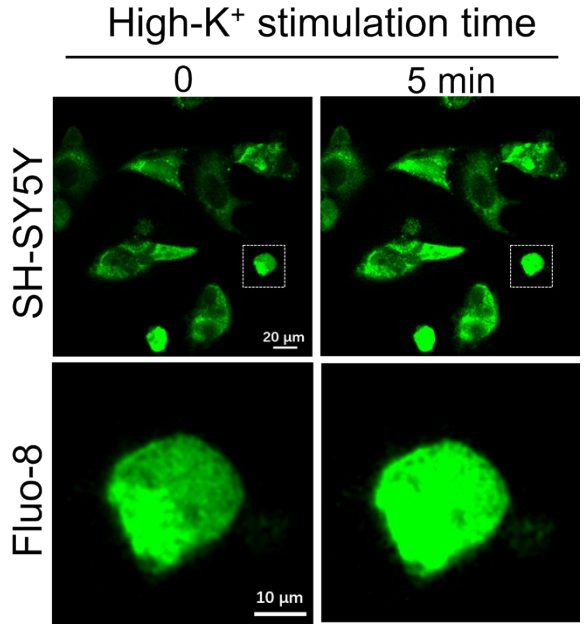

Figure S9. Time-lapse confocal imaging of SH-SY5Y cells with or without High-K^+ buffer stimulation and then incubated with 5 μM Fluo-8, scale bar: 20 μm. The zoom-in images are lighted by 5 μM Fluo-8 to trace the calcium flux, scale bar: 10 μm.

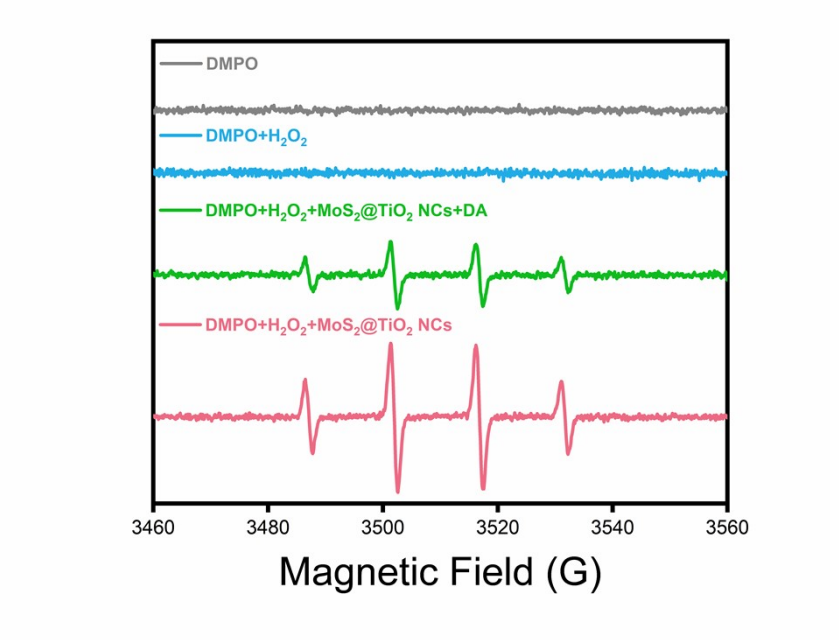

Figure S10. EPR measurement of captured ·OH that catalyzed by MoS_2@TiO_2 NCs and the ·OH competition by DA.

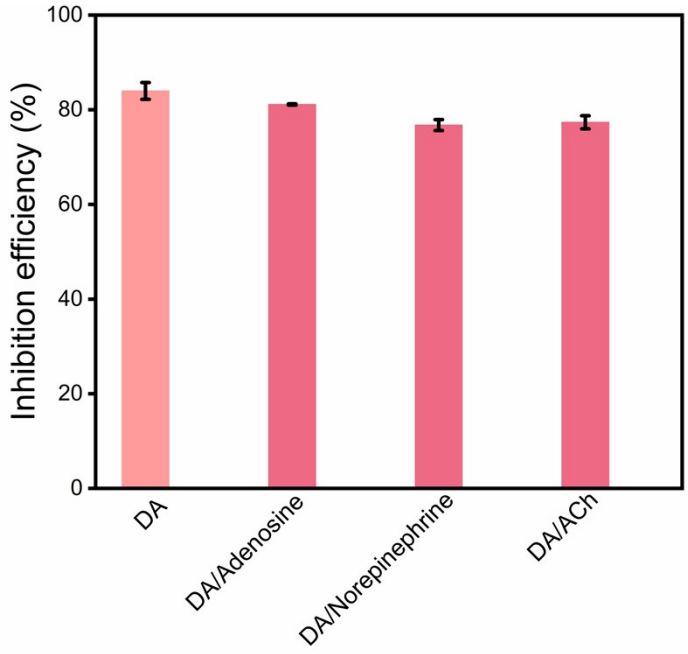

Figure S11. The inhibition efficiency of DA with coexisting other types of neurotransmitters, the concentration of DA and the other neurotransmitters are 200 μM.

References:

Fan, K., Wang, H., Xi, J., Liu, Q., Meng, X., Duan, D., Gao, L., Yan, X., 2016. Optimization of Fe_3O_4 nanozyme activity via single amino acid modification mimicking an enzyme active site. Chem Commun (Camb) 53(2), 424-427. https://doi.org/10.1039/c6cc08542c

Feng, J.J., Guo, H., Li, Y.F., Wang, Y.H., Chen, W.Y., Wang, A.J., 2013. Single molecular functionalized gold nanoparticles for hydrogen-bonding recognition and colorimetric detection of dopamine with high sensitivity and selectivity. ACS Appl Mater Interfaces 5(4), 1226-1231. https://doi.org/10.1021/am400402c

He, Y., Li, N., Liu, X., Chen, W., Zhu, X., Liu, Q., 2021. 5,10,15,20-tetrakis (4-carboxyl phenyl) porphyrin-functionalized urchin-like $CuCo_2O_4$ as an excellent artificial nanozyme for determination of dopamine. Mikrochim Acta 188(5), 171. https://doi.org/10.1007/s00604-021-04819-9

Liu, H., Ding, Y.N., Bian, B., Li, L., Li, R., Zhang, X., Liu, Z., Zhang, X., Fan, G., Liu, Q., 2019. Rapid colorimetric determination of dopamine based on the inhibition of the peroxidase mimicking activity of platinum loaded $CoSn(OH)_6$ nanocubes. Mikrochim Acta 186(12), 755. https://doi.org/10.1007/s00604-019-3940-5

Rithesh Raj, D., Prasanth, S., Vineeshkumar, T.V., Sudarsanakumar, C., 2016. Surface plasmon resonance based fiber optic dopamine sensor using green synthesized silver nanoparticles. Sensors and Actuators B: Chemical 224, 600-606. https://doi.org/10.1016/j.snb.2015.10.106

Wang, J., Du, R., Liu, W., Yao, L., Ding, F., Zou, P., Wang, Y., Wang, X., Zhao, Q., Rao, H., 2019. Colorimetric and fluorometric dual-signal determination of dopamine by the use of Cu-Mn-O microcrystals and C-dots. Sensors and Actuators B: Chemical 290, 125-132. https://doi.org/10.1016/j.snb.2019.03.107

Wen, F., Jiang, T., He, L., Su, J., Jiang, P., He, D., Chen, Z., 2022. Ru incorporation for boosting Co_3O_4 oxidase-like activity in dopamine colorimetric detection. Applied Surface Science 603, 154434. https://doi.org/10.1016/j.apsusc.2022.154434